NASA Technical Memorandum 86897

Creep of Chemically Vapor Deposited SiC Fibers

James A. DiCarlo
Lewis Research Center
Cleveland, Ohio

Prepared for the
Eighth Annual Conference on Composites and
Advanced Ceramic Materials
sponsored by the American Ceramic Society
Cocoa Beach, Florida, January 15–18, 1984

NASA

CREEP OF CHEMICALLY VAPOR DEPOSITED SiC FIBERS

James A. DiCarlo
National Aeronautics and Space Administration
Lewis Research Center
Cleveland, Ohio 44135

SUMMARY

The creep, thermal expansion, and elastic modulus properties for chemically vapor deposited SiC fibers were measured between 1000 and 1500° C. Creep strain was observed to increase logarithmically with time, monotonically with temperature, and linearly with tensile stress up to 600 MPa. The controlling activation energy was 480±20 kJ/mole. Thermal pretreatments near 1200 and 1450° C were found to significantly reduce fiber creep. These results coupled with creep recovery observations indicate that below 1400° C fiber creep is anelastic with negligible plastic component. This allowed a simple predictive method to be developed for describing fiber total deformation as a function of time, temperature, and stress. Mechanistic analysis of the property data suggests that fiber creep is the result of β-SiC grain boundary sliding controlled by a small percent of free silicon in the grain boundaries.

INTRODUCTION

Substantial interest in continuous silicon carbide (SiC) fibers has developed recently because of their potential as reinforcement for high temperature ceramic matrix composites. As a strong, stiff, and thermally stable material, the SiC fiber should add not only strength and stiffness to a ceramic matrix but also improved fracture toughness. The mechanisms for toughening are many and strongly dependent on the deformation and fracture properties of both composite constituents (ref. 1). Thus the need arises for measuring and understanding the mechanical properties of SiC fibers, especially at high temperature where significant deviation from low temperature behavior can occur.

The primary objective of the present study was to determine the creep deformation behavior of SiC fibers produced commercially by chemical vapor deposition (CVD). These fibers were chosen because in their as-produced state they offer significantly greater strength and modulus than continuous SiC fibers produced by other methods, such as, polymer pyrolysis (ref. 2). The experimental approach was to apply a constant axial load to a long length fiber and then resistance heat the fiber in an inert atmosphere at temperatures in the range 1000 to 1500° C. The advantages of this test approach were many. First, it allowed measurements of fiber creep strain as a function of time, temperature, and stress. Second, the use of tensile stress and long fiber length simplified deformation analysis and permitted high sensitivity strain measurements. Third, the resistance heating method permitted direct and rapid temperature control and uniform temperatures along long fiber lengths. Last, but not least, the test method also allowed time-independent fiber thermal expansion and elastic modulus data to be obtained.

EXPERIMENTAL

Specimens

The SiC fiber specimens were obtained commercially from Avco Specialty Materials Division. The basic fiber production method involved the chemical decomposition of a silane-hydrogen gas mixture onto a resistively-heated graphite-coated carbon monofilament which passed continuously through a CVD reactor (ref. 3). For optimum fiber tensile strength, the deposition temperature profile within the reactor decreased from ~1300° C at fiber entrance to ~1150° C at fiber exit.

The result of the SiC deposition is shown schematically in figure 1(a). The filament cross section displays a SiC sheath with an outer diameter of 142 μm surrounding an unreacted graphite-coated carbon core with an outer diameter of ~37 μm. The sheath microstructure consists of β-SiC columnar grains extending in the radial direction with <111> preferred orientation and lengths of a few micrometers (ref. 4). At a radius of ~40 μm, a distinct change in microstructure can be optically observed within the sheath. Associated with this change is an abrupt increase in average grain diameter from ~50 nm in the inner region A to ~100 nm in the outer region B (ref. 4). This transition is the result of temperature and gas compositional differences from the entrance to the center of the reactor.

Because of the deposition conditions, it was anticipated that the CVD SiC sheath should also contain small percentages of free silicon and carbon (ref. 5). X-ray microprobe scans across the fiber cross section showed that the silicon to carbon ratio increased in passing from region A to B. This observation coupled with the lower deposition temperature for region B suggests that this region contained free silicon. This conclusion is in agreement with the phase analysis results of Martineau et al. (ref. 6) who found that region A generally contained a few percent excess carbon whereas region B was either stoichiometric or slightly silicon rich.

To improve and maintain fiber strength, the manufacturer typically deposits thin silicon-containing carbon-rich coatings onto the SiC fiber surface. Schematic representations of the silicon content in the coatings for the two fiber types employed in this study are shown in figures 1(b) and 1(c). The coating for the standard SiC fiber (cf. fig. 1(b)) is graded in composition from amorphous carbon on the outside to approximately stoichiometric SiC at a depth of ~1 μm (ref. 7). The ~2 μm thick coating for the SCS-6 fiber (cf. fig. 1(c)) consists of essentially pure amorphous carbon covered by a carbon-rich overlayer containing silicon in both the α and β-SiC crystalline forms (refs. 4 and 8). Average as-received tensile strengths for the standard SiC and SCS-6 fibers in this study were 5.5 and 4.3 GPa, respectively.

Although some fiber properties such as tensile strength can depend strongly on the carbon-rich coatings and the carbon core (ref. 9), fiber creep, thermal expansion, and elastic modulus should be controlled only by the SiC sheath. That is, under axial deformation conditions, negligible stress should be carried by the coatings or core because their maximum volume fractions are only 3 and 7 percent, respectively, and also because their moduli are significantly less than that of the SiC sheath. Indeed, the results of this study detected no deformation property differences between the standard

SiC and SCS-6 fibers even though their surface coatings were greatly different in microstructure and volume fraction.

Procedure

The apparatus employed for the high temperature deformation tests (ref. 10) is similar to a commercial CVD reactor in which a long length of fiber (~600 mm) is resistance heated within a controlled gaseous environment. Water-cooled stainless steel caps at each end of a 25 mm diameter glass tube contain inlet and outlet gas ports and mercury seals for electrical contact to the fiber. Test runs were performed in one atmosphere of nominally pure argon (0.01 percent oxygen volume fraction) flowing through the tube at 200 cc/min.

Axial tensile stresses were achieved by clamping the fiber above the top end cap and adding various clamp loads below the lower cap. Traveling microscopes located at the clamps were used to measure deformations with an accuracy of ±10 μm. Strain was calculated as the ratio of deformation to fiber length. For convenience, the applied tensile stress was calculated assuming the entire fiber cross section carried the load. Thus listed stresses may underestimate the true sheath stresses by as much as 10 percent, assuming coating and core carried no load.

Fiber temperature was determined at the fiber center by optical pyrometer measurements corrected for fiber emmissivity, glass transmission losses, and temperature gradients along the fiber. Average total emmissivity values calculated from electrical power input data were 0.66 and 0.75 for the standard SiC and SCS-6 fibers, respectively. Temperature differences between the fiber center and the ends of the heated fiber section were small, reaching a maximum of 30° C at 1500° C. The error in the final temperature determination was estimated at ±10° C. Above 1450° C, active oxidation effects (ref. 11) began to remove surface coatings and reduce fiber diameter. This problem limited test temperatures to a maximum of 1500° C.

For a typical test run, the initial procedure was to pretreat the fiber at a given temperature for 30 min. This was accomplished by clamping the fiber under minimal load (9 g) to achieve straightness and then increasing dc current to a preset value which was held constant throughout the run. Thermal equilibrium conditions were attained in ~5 min allowing accurate measurements of fiber thermal expansion.

Following the pretreatment run, loads ranging from 450 to 1000 g were applied at room temperature. The resulting deformation was used to determine the 20° C elastic modulus, E_o. Loads larger than 1000 g were attempted, but this usually resulted in fiber fracture either upon loading at room temperature or upon reaching test temperature. The sources of fracture were not examined. The fiber was then rapidly heated (~10 sec) to the same pretreatment temperature where a time-dependent creep deformation was observed and measured. After 30 min or more, current was quickly (~10 sec) decreased to zero, leaving a residual creep strain in the fiber. The length change upon cooling was slightly larger by ΔL than the fiber expansion previously measured during the pretreatment run. This reflects a smaller fiber elastic modulus at the test temperature than at 20° C. The modulus ratio E/E at temperature was calculated from

$$\frac{E}{E_0} = \left[1 + \frac{E_0 \Delta L}{\sigma L}\right]^{-1} \qquad (1)$$

where σ is the applied stress and L the heated fiber length.

In some cases, creep runs were performed on as-received fibers with no preceeding thermal pretreatment. Also, in a few instances, specimens with developed creep strains were reheated under minimal load (9 g) to the same or to a higher test temperature in order to measure creep recovery as a function of time. In some situations, creep and creep recovery tests were repeated two or three times on the same specimen.

RESULTS

Creep

Typical fiber creep curves for various temperatures and a stress of 278 MPa are shown in figure 2. For time periods ranging up to a few hours, the creep curves were found to follow very nearly a logarithmic dependence on time. This indicates that the microstructural imperfections responsible for creep became limited in motion due to the buildup of internal stresses. If imperfection motion is reversible, then applied stress removal should allow the internal stresses to force the imperfections back to their original positions, provided temperature is high enough to activate motion. As such, creep recovery would be observed and fiber deformation would be classified as anelastic or recoverable (ref. 12).

The fact that SiC fiber creep deformation is indeed anelastic is demonstrated by the creep and creep recovery curves of figure 3. Turning first to figure 3(a), one finds that over 60 percent of the strain developed in 30 min at 1180° C and 278 MPa was recovered in 150 min at the same temperature and zero load. The trend of the curve suggest that further recovery would have occurred beyond 150 min but the time required for almost complete recovery would have been considerably large. However, since creep is controlled by thermally-activated motion, recovery should be quicker if the recovery temperature is allowed to be greater than the test temperature. This fact is clearly shown by the curves of figure 3(b) where over 90 percent of creep strain developed in 30 min at 1275° C was recovered in a similar time at 1450° C.

Besides demonstrating thermally activated creep recovery, the curves of figure 3 also show an interesting result concerning high temperature mechanical fatigue of the fibers. For example, figure 3(a) indicates that at 1180° C, a tension-tension fatigue condition of 30 min with stress and 150 min without stress resulted in no cummulative increase in fiber creep strain. Indeed, residual strain actually decreased during cycling. A similar result is evident in figure 3(b) where the zero-load temperature was higher than the loading temperature. Certainly if the fiber creep strain contained any plastic or permanent deformation component, repeated cycling in the tension-tension mode should produce a net increase in strain. Thus it follows that at these stress and temperature conditions, CVD SiC fiber creep is entirely anelastic.

It should be made clear that the figure 3 curves showing no increase in residual creep strain during cycling is a consequence of the recovery time-temperature cycle employed. Obviously, if the recovery cycle had a zero time duration, creep strain would continue to increase, following nearly a log time dependence.

Another important property characteristic of anelastic deformation is a linear dependence between creep strain ε_c and applied stress σ, or a creep compliance $J_c = \varepsilon_c/\sigma$ which is only time and temperature dependent and stress independent. In order to demonstrate stress independence for the fiber J_c as well as indicate the strong effects of thermal pretreatment on fiber creep, the creep compliance data measured after 30 min, J_c (30), were plotted in figure 4 as a function of test temperature. The applied stress levels and thermal pretreatment conditions are distinguished by the notation in the figure legend. Three pretreatment ranges are identified: 1150 to 1360° C, 1400 to 1500° C, and as-received or no thermal pretreatment. Data for the SCS-6 fiber are underlined.

Examining first the open symbols for pretreatment temperatures between 1150 and 1360° C, one finds that all the J_c (30) data for the two fiber types fall very nearly on the same curve b. Since these data represent stresses ranging from 278 to 612 MPa, it follows that below 600 MPa, J_c is independent not only of fiber coating but also of stress. When the pretreatment temperature was increased above 1400° C, the solid data points show that a definite reduction in creep occurred across a wide temperature range. This dropoff further continued as pretreatment temperatures approached 1500° C. Apparently during pretreatment runs above 1400° C, microstructural changes occurred with the CVD fiber sheath which somehow reduced imperfection motion during the subsequent creep runs.

Finally, turning to the no pretreatment (tailed) data of figure 4, one finds two stress-independent points at 1200° C which are measurably greater than the curve b data and three points above 1200° C which fall on curve b. (The curve a extrapolation of the 1200° C data to lower temperatures will be explained shortly). These results suggest thermally-induced microstructural changes that reduce creep also occurred between 1200 and 1300° C as well as above 1400° C. That is, upon direct loading to 1200° C (or below), imperfections whose motion would otherwise be hindered by pretreatment runs near 1200° C were still available to participate in creep. Thus as-received creep up to 1200° C was greater than creep after pretreatment. However, upon direct loading to 1300° C and above, motion of these same imperfections became hindered because the 1200° C annealing temperature had been sufficiently exceeded. A similar argument can be used to explain why the as-received data above 1400° C were measurably higher than the 1400° C pretreatment data.

Creep Analysis

The fact that time-dependent deformation below 1400° C can be classified as anelastic allows SiC fiber creep to be phenomenologically analyzed and functionally described in terms of time, temperature, and stress without any knowledge of the exact underlying physical mechanisms. This convenience is of practical significance since it implies that fairly accurate predictions of total fiber deformation can be made for test conditions not included in the experimental data.

In anelastic theory (ref. 12), the total creep strain is the result of the cummulative motion of many small microstructural imperfections which move or relax at different times due to a distribution in relaxation times τ. Generally, as in the case for the SiC fiber, imperfection motion is thermally-activated so that relaxation times decrease with increasing temperature according to the Arrhenius equation

$$\tau = \tau_0 \exp\left[\frac{Q}{RT}\right] \quad . \tag{2}$$

Here the activation energy Q is the height of the thermal barrier for relaxation, R is the gas constant, T is the absolute temperature, and

$$\tau_0 = (2\pi \nu_0)^{-1} \tag{3}$$

where ν_0, the attempt frequency, is the number of times per second the relaxing imperfection attempts to cross the barrier.

The observation of logarithmic creep indicates that there are many relaxing imperfections participating in SiC fiber creep and that the relaxation times are broadly distributed due to a broad distribution in τ_0 or Q or in both parameters. In this situation it is convenient to invoke the broad distribution approximation (ref. 12). Under this approximation, an imperfection with relaxation time τ moves when $\tau = t$ so that by equation (2),

$$\ln t = \ln \tau_0 + \frac{Q}{RT} \quad . \tag{4}$$

To ascertain whether the relaxation times were distributed in τ_0 or Q, the cross-cut method for determining activation energy Q was applied to the time-dependent creep curves measured in the 1150 to 1360° C pretreatment range. For this method, the log of the test time t required to achieve a certain strain level was plotted in figure 5 against the reciprocal test temperature. By equation (4), the Q of the last imperfection to relax can be determined from the slope of the resulting straight line.

Examination of the best fit lines of figure 5 show that up to 1360° C, Q did not increase with creep strain but remained fairly constant at a value of 480±20 kJ/mole. It can be assumed then that a broad distribution in τ_0 is the only source for the distribution in relaxation times. Letting $\gamma \equiv \ln \tau_0$, it follows by equation (4) that creep strain observed at test temperature T after time t (sec) is the result of the cummulative motion of imperfections with γ values equal or less than

$$\gamma = \ln t - \frac{57\,700}{T} \quad . \tag{5}$$

Here Q/R has been replaced by the experimental value determined from figure 5.

In light of the above analysis, fiber creep compliance J_c can be considered a function only of the relaxation parameter γ which is dependent on test time and temperature by the equation (5) relationship. Thus if J_c is measured at a certain γ value, that same J_c will occur at any combination

of time and temperature that gives the same γ value. It follows then that creep strain is predictable from

$$\varepsilon_c = \sigma J_c(\gamma) \tag{6}$$

where $J_c(\gamma)$ is an experimentally measurable function. To determine $J_c(\gamma)$ for the SiC fiber, the 30 min compliance results of figure 4 were employed to yield the three curves of figure 6. Curve a of figures 4 and 6 was constructed using equation (6) and the short time creep data for the as-received 1200° C specimens.

In conclusion, for temperatures below 1400° C and stresses below 600 MPa, the elastic and anelastic nature of CVD SiC fiber deformation allows one to make fairly accurate predictions of total fiber strain ε as a function of time, temperature, and stress; i.e.,

$$\varepsilon = \varepsilon_e + \varepsilon_c + \varepsilon_T = \frac{\sigma}{E} + \sigma J_c(\gamma) + \varepsilon_T \tag{7}$$

Here ε_e is the elastic strain component and ε_T the thermal expansion strain. It should be noted that for very long periods of time at constant temperature, $J_c(\gamma)$ varies slowly with time ($\sim t^{1/3}$) so that steady state creep rates do not exist for the anelastic CVD SiC fiber, at least below 1400° C.

Thermal Expansion

The thermal strain results for both types of CVD SiC fiber are given in figure 7. For warmups below 1350° C, strain increased in a nearly linear manner and was reproducible during cooldown. These data are in good agreement with the results of Kern et al. for bulk CVD SiC (ref. 13). For warmups above 1360° C, however, the fiber thermal strain was observed to drop abruptly. As shown in figure 7, this contraction began near 1360° C and ended near 1390° C, amounting to an average strain decrease of 0.04 percent. Above 1400° C the thermal strain during warmup followed a curve parallel to the extension of the lower temperature curve.

On cooldown from above 1400° C, thermal strain followed the high temperature warmup curve until 1330° C where it began to increase. At 1280° C this small expansion was complete and the cooldown curve followed the original low temperature curve down to room temperature. A similar hysteretic effect was also observed by Kern et al. (ref. 13) who suggested free silicon as the source. This conclusion was based on the fact that on melting near 1400° C, silicon contracts when going from the solid to the liquid phase (ref. 14).

Careful monitoring of the fiber length at room temperature revealed a reproducible residual strain after the first thermal cycle above 1400° C. The 20° C tensile strain shown in figure 8 was measured after a 30 min thermal treatment at the indicated temperature followed by a rapid quench to room temperature. From comparison with the figure 7 data, it can be concluded that this effect was probably caused by the contraction mechanism operating near 1400° C. That is, quenching the fiber after a 1400° C treatment resulted in a 20° C contraction which began to recover during thermal treatment near 1200° C. As the treatment temperature progressed above 1200° C, the recovery continued

to occur until 1400 °C where the contraction mechanism was allowed to operate again so that the entire process could be repeated.

Elastic Modulus

The 20° C axial elastic modulus results for the standard SiC fibers are given in table I. Included in this table are the moduli measured under static tension in this study and under dynamic flexure in a previous study (ref. 15). The slight difference in modulus results is to be expected since the tension method senses both the high modulus SiC sheath and the low modulus carbon core whereas the flexure method primarily senses the outer surface layers of the sheath. Accounting for the effects of core and coating for each test method (ref. 15), one can calculate sheath modulus values in fairly good agreement (cf. table I).

The temperature dependence for the elastic modulus of the standard SiC fiber is shown in figure 9. The high temperature data points with large scatter were measured by static tension using equation (1). The scatter arose from a lack of sufficient experimental resolution in length measurement ΔL rather that real physical differences among the specimens. The more accurate low temperature data shown by the continuous curve were measured previously using the sheath-sensitive dynamic flexure method (ref. 15).

DISCUSSION

Because the CVD SiC fiber creep observed in this study is anelastic or recoverable and occurs at temperatures where dislocation motion is negligible (ref. 16), the controlling creep mechanism can be identified as grain boundary sliding (GBS) in which β-SiC grains under applied stress and high temperature move or slide with respect to their neighbors. Due to the buildup of elastic stresses at grain boundary intersections, the GBS process becomes limited in time, giving rise to creep saturation effects (cf. fig. 2). When the applied stress is removed, the internal stresses force the grains to slide back to their original position, resulting in macroscopic creep recovery.

Zener's theory for GBS (ref. 17) predicts that at the completion of grain motion, J_c for the SiC fiber should saturate at a value of 1.5×10^{-12} Pa^{-1}. Clearly the J_c results of figure 6 show much higher values with no evidence of saturation to at least 1450° C. Although there are many creep situations in which Zener's theory is indeed obeyed, there are also others in which experimental creep strains exceed his predictions (ref. 12). As is the case for the CVD fiber, these large strains remain anelastic in that they are directly proportional to stress and can be recovered by stress removal.

One model that can be invoked to explain the large anelastic creep strains is that after simple motion of single grains as predicted by Zener, there can occur more complicated motion in which a set of multiple grains moves with respect to another set of multiple grains. Because the attempt frequency (cf. eq. (3)) for multiple grain motion should be less than that for single grain motion, the distribution for GBS creep should begin at the single grain τ_o and extend to larger and larger τ_o for multiple grain motion. In this regard, it is interesting to note that the $\ln \tau_o$ value typically observed for Zener single grain motion is $\ln 10^{-15}$ or -35, a value in good agreement

with the γ in figure 6 where significant creep effects are first observed in the SiC fiber.

Turning to the mechanism controlling grain motion, it has been generally observed that for those creep situations with GBS as the accepted source, the activation energy controlling creep agreed closely either with the lattice self-diffusion energy or the grain-boundary self-diffusion energy of the particular material or with the lattice self-diffusion energy of impurity phases in the grain boundaries. A physical model for this correlation is that the viscosity of the interfacial boundary layer between grains is controlled by diffusion mechanisms in the layer (ref. 12). Assuming this to be the case for the SiC fiber, one would then expect the measured creep activation energy of 480±20 kJ/mole to possibly agree with the self-diffusion or grain boundary diffusion energies of either Si or C in polycrystalline β-SiC or with the self-diffusion energy of free silicon since this metal, as discussed earlier, can exist to some degree within the CVD fiber. Comparing the literature values for these energies, given in table II, with the creep energy of this study, one finds little agreement with the β-SiC values but excellent agreement with the silicon metal value. This observation suggests that β-SiC grain boundary sliding in the CVD fiber is controlled by free silicon metal located within the grain boundaries.

Additional evidence for the presence of free silicon between β-SiC grains can be found in the decrease in thermal expansion strain observed near 1380° C during warmup (cf. fig. 7). As suggested by Kern et al. (ref. 13), this effect can be explained by the 9 percent reduction in volume (ref. 14) displayed by silicon metal when it changes from solid to liquid. Assuming that the observed fiber axial contraction of 0.04 percent occurred uniformly in all directions, and that the free silicon located between β-SiC grains contracted fully on melting, one estimates that V_{Si}, the average volume fraction of free silicon in the CVD fiber, is ~1.4 percent. However, the large aspect ratio of the β-SiC grains and their preferred radial orientation suggests that silicon contraction should only be observed in the axial and tangential directions, so that a better estimate for V_{Si} under full contraction is ~1 percent.

The 1 percent value for silicon content should be considered a lower limit because full silicon contraction was most likely prevented by internal constraints. Indeed, the difference between the normal pressure silicon melting temperature (1410° C) and the temperature for contraction on warmup (1380° C) and for expansion on cooldown (~1310° C) suggest by Clapeyron's equation that the excess silicon was under large internal compression (~1 GPa). Such high internal stress could have been generated by growth mechanisms during CVD (ref. 5) or possibly by the thermal expansion mismatch between the silicon and β-SiC.

At this point, one might compare the present creep results with literature data for other types of SiC ceramics at temperatures below 1500° C. This comparison is difficult in most cases because the creep data is usually presented in terms of "steady state creep rates" which, as discussed earlier for anelastic creep, may actually be time dependent. A more accurate comparison would be in terms of total creep strain measured under similar time, temperature, and stress conditions. Such total creep strain measurements have been made by Marshall and Jones for reaction-bonded or siliconized SiC (Refel) containing ~10 percent free silicon (ref. 20). As shown by the solid data points of figure 5, their results are in good agreement with the CVD fiber

data. This close similarity in creep magnitude and activation energy is considered strong evidence for grain boundary silicon as the controlling GBS phase for both types of SiC materials. (The often quoted activation energy of 230 kJ/mole measured by Marshall and Jones is believed to be incorrect due to their questionable energy determination method).

Regarding silicon-free sintered SiC ceramics, higher test temperatures are generally required to observe creep rates equivalent to those of silicon-ized SiC (ref. 21). Since the sintered materials typically contain free carbon in the grain boundaries, these results suggest that GBS does occur in sintered SiC but, rather than silicon, carbon with its higher activation energy (cf. table II) may be the creep controlling intergranular phase.

Comparing CVD SiC fiber creep with that of the polymer-derived Nicalon SiC fiber (ref. 22), one finds almost an order of magnitude lower creep strain for the CVD fiber under similar test conditions. This can be explained possibly by the lower viscosity silicon-oxide phase known to created in the Nicalon fiber during its production (ref. 2).

One final point that should be addressed is the possible sources for the creep reductions observed in the CVD fiber after thermal pretreatments near 1250 and 1450° C. In light of the above GBS model, a reduction in creep could be explained by (I) a decrease in the number of grains available for sliding or (II) an increase in the viscosity of the grain boundary material. Process I may typically occur by grain lockup in which stress-driven motion during pretreatment places some grains in new locations where they are unable to move until applied stresses reach levels greater than those required for grain motion prior to pretreatment. Process II may occur by the removal of the grain boundary material or by the addition of higher viscosity phases to the boundaries. Under this condition higher stresses should not be able to restore creep behavior.

Because below 1400° C the free silicon remains intact within the grain boundaries, the 1250° C pretreatment effect was probably caused by process I. That is, under zero external load conditions, some of the grains moved to new positions where they became locked with respect of maximum stress levels of this study (600 MPa). The internal driving force for this grain motion was probably residual growth stresses in the outer sheath layers which were not fully relieved during the CVD process because the time-temperature conditions during deposition were lower than those applied during pretreatment.

On the other hand, the 1450° C pretreatment effect occurred in a temperature region where effects from both processes I and II might be expected to operate. For example, internal stresses generated near 1400° C by the contraction effect might be expected to move grains into new and possibly locked positions. Also, near 1450° C, free silicon in liquid form might be expected to diffuse rapidly and be removed from the boundaries possibly by reaction with free carbon within the fiber sheath. As described above, the application of high stresses after pretreatment could clarify the responsible creep reduction mechanism. However, at these temperatures there is a considerable loss in fiber tensile strength (refs. 9 and 23) which significantly limits the applied creep stress. Thus, at the present time the mechanism for the 1450° C pretreatment effect remains uncertain. Nevertheless, the fact that this effect occurs near the silicon melting point is additional strong evidence for the presence of this metal in free form.

CONCLUDING REMARKS

The deformation property results of this study indicate that the sheath of the commercial CVD SiC fiber is a composite in itself, consisting of β-SiC grains with a small percent of free silicon metal in the grain boundaries. Whereas the fiber modulus and thermal expansion strain are essentially controlled by the β-SiC grains, fiber creep below 1400° C appears to be the result of grain boundary sliding controlled by the free silicon. As such, the CVD fiber displays creep characteristics similar to bulk SiC ceramics that are produced with excess silicon in their microstructure. Although fiber creep below 1400° C is greater than that of silicon-free SiC ceramics, its anelastic nature does allow the possibility of creep recovery and also the practical convenience of utilizing simple relaxation theory to predict total creep strain as a function of time, temperature, and stress.

Thermal pretreatment of the CVD fiber at temperatures greater than 1400° C was observed to significantly increase fiber creep resistance, suggesting that some loss of free silicon may have occurred. Although this may appear to be a practical means for improving high temperature deformation behavior, these thermal treatments have also been observed to cause a measurable loss in fiber tensile strength. In like manner, for CVD temperatures greater than 1300° C where the likelihood of free silicon formation is reduced, the fiber manufacturer has found less than optimum tensile strength for the as-produced fibers. These results suggest that although the free silicon may be somewhat detrimental to fiber creep deformation, its presence may be unavoidable if one desires high fiber tensile strength, a property of prime importance for the structural performance of ceramic composites. Indeed, the fundamental question arises whether excess silicon may in fact be a requirement for high fiber strength.

REFERENCES

1. R.W. Rice, "Mechanisms of Toughening in Ceramic Matrix Composites," Ceram. Eng. Sci. Proc., 2 [7-8] 661-701 (1981).

2. S. Yajima, "Special Heat-Resisting Materials from Organometallic Polymers," Am. Ceram. Soc. Bull. 62 [8] 893-903 (1983).

3. H. Debolt and V. Krukonis, "Improvement of Manufacturing Methods for the Production of Low Cost Silicon Carbide Filament," Air Force Contract F33615-72-C-1177, Report No. AFML-TR-73-140, September 1973.

4. F.W. Wawner, A.Y. Teng, and S.R. Nutt, "Microstructural Characterization of SiC (SCS) Filaments," SAMPE Q. 14 [3] 39-45 (1983).

5. J.R. Weiss and R.J. Diefendorf; pp. 488-497 in Chemical Vapor Deposition Edited by G. Wakefield and J.M. Blocher, Jr., Electrochem Soc., Princeton, N.J., 1973.

6. P. Martineau, M. Lahaye, R. Pailler, R. Naslain, M. Couzi, and F. Creuge, "SiC Filament/Titanium Matrix Composites Regarded as Model Composites, J. Mater. Sci. 19 [8] 2731-2748 (1984).

7. J.A. Cornie, R.J. Suplinskas, and A.W. Hauze, "Filament Surface Enhancement for Casting and Hot Molding SiC/Al Composites," Ceram. Eng. Sci. Proc., 1 [7-8] 728-743 (1980).

8. R.J. Suplinskas, and H. Debolt, "Surface Enhancement of Silicon Carbide Filament for Metal Matrix Composites," ONR Contract N00014-79-C-0691, 1981. (AD-A110780.)

9. T. Bhatt, "Environmental Effects on the Tensile Strength of Chemically Vapor Deposited Silicon Carbide Fibers," J. Mater. Sci., to be published.

10. J.A. DiCarlo and T.C. Wagner, "Oxidation-Induced Contraction and Strengthening of Boron Fibers," Ceram. Eng. Sci. Proc., 2 [7-8] 872-893 (1981).

11. E.A. Gulbransen and S.A. Jansson, "The High Temperature Oxidation, Reduction, and Volatilization Reactions of Silicon and Silicon Carbide," Oxid. Met., 4 [3] 181-201 (1972).

12. A.S. Nowick and B.S. Berry, Anelastic Relaxation in Crystalline Solids, Academic Press, New York, 1972.

13. E.L. Kern, D.W. Hamill, H.W. Diem, and H.D. Sheets, "Thermal Properties of β-Silicon Carbide from 20 to 2000 °C," Mat. Res. Bull., 4, S25-S32, (1969).

14. R.A. Logan and W.L. Bond, "Density Change in Silicon Upon Melting," J. Appl. Phys., 30 [3] 322 (1959).

15. J.A. DiCarlo and W. Williams, "Dynamic Modulus and Damping of Boron, Silicon Carbide, and Alumina Fibers," Ceram. Eng. Sci. Proc. 1 [7-8] 671-692 (1980).

16. P.L. Farnsworth and R.L. Coble, "Deformation Behavior of Dense Polycrystalline SiC," J. Am. Ceram. Soc., 49 [5] 264-268 (1966).

17. C. Zener, "Theory of the Elasticity of Polycrystals with Viscous Grain Boundaries," Phys. Rev., 60 [12] 906-908 (1941).

18. M.H. Hon, R.F. Davis, and D.E. Newbury, "Self-Diffusion of ^{30}Si in Polycrystalline β-SiC," J. Mater. Sci., 15 [8] 2073-2080 (1980).

19. Metals Reference Book, 5th edited by C.J. Smithells and E.A. Brandes, Butterworths, London, 1976.

20. P. Marshall and R.B. Jones, "Creep of Silicon Carbide," Powder Metall., 12 [23] 193-208 (1969).

21. D.C. Larsen and J.W. Adams, "Property Screening and Evaluation of Ceramic Turbine Materials," Air Force Contract F33615-79-C-5100, Report No. AFWAL-TR-83-4141, April 1984.

22. G. Simon and A.R. Bunsell, "The Creep of Silicon Carbide Fibers," J. Mater. Sci. Lett. 2 [2] 80-82 (1983).

23. I. Ahmad, D.N. Hill, J. Barranco, R. Warenchak, and W. Heffernan; pp. 156-174 in Advanced Fibers and Composites for Elevated Temperatures, edited by I. Ahmad and B.R. Noton, The Metallurgical Society of AIME, Warrendale, Pa., 1980.

TABLE I. - SiC FIBER MODULUS AT 20° C

		Fiber (measured)	Sheath (calculated)[a]
Modulus, GPa	Axial static	391±5	427±5
	Flexural dynamic	[b]414±9	436±9

[a]Using properties from reference 15.
[b]Reference 15.

TABLE II. - ACTIVATION ENERGIES FOR SELF-DIFFUSION

		Lattice, kJ/mole	Grain-boundary, kJ/mole
β-SiC[a]	Silicon	912±5	-----
	Carbon	841±14	564±9
Silicon metal[b]		494±10	-----
		460	-----

[a]Reference 18.
[b]Reference 19.

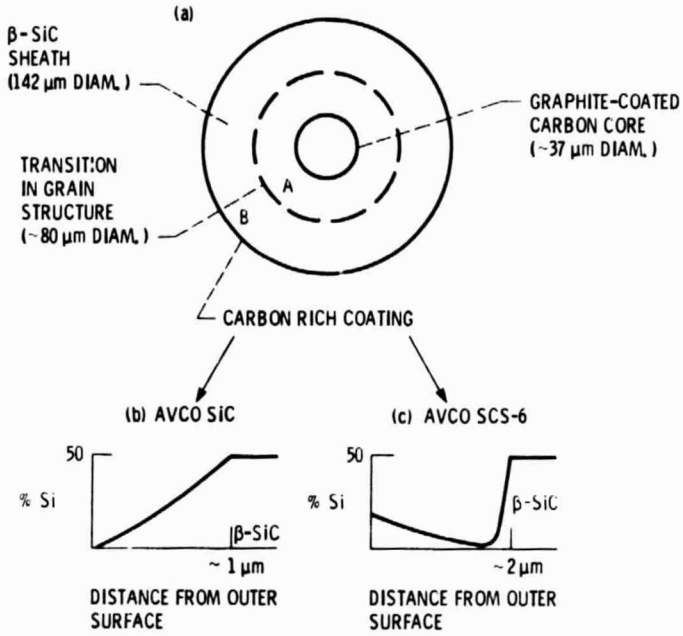

Figure 1. - Schematic representations of (a) the CVD SiC fiber cross section and (b and c) the silicon content in the two types of carbon-rich fiber coatings.

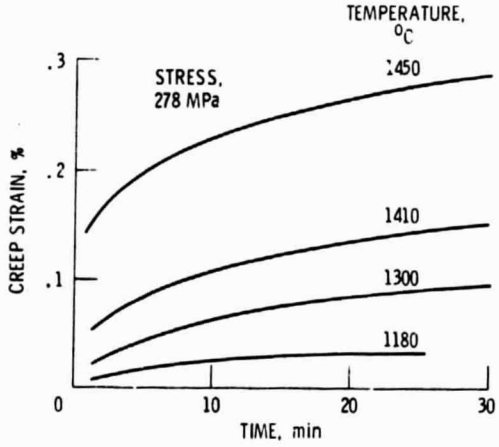

Figure 2. - Typical creep data for CVD SiC fibers.

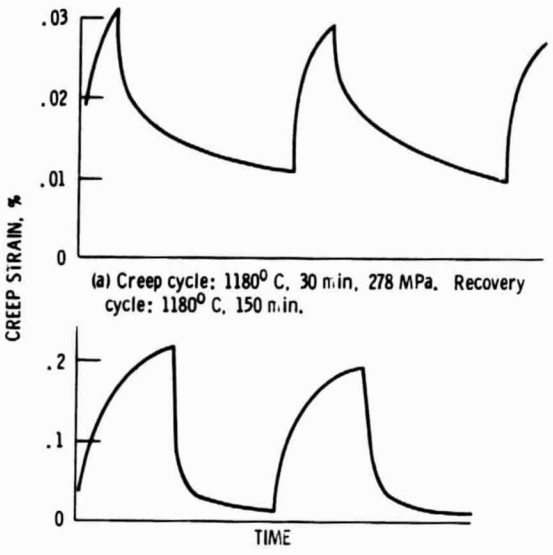

(a) Creep cycle: 1180° C, 30 min, 278 MPa. Recovery cycle: 1180° C, 150 min.

(b) Creep cycle: 1275° C, 30 min, 612 MPa. Recovery cycle: 1450° C, 30 min.

Figure 3. - Creep and creep recovery curves for repeated load/no-load cycles.

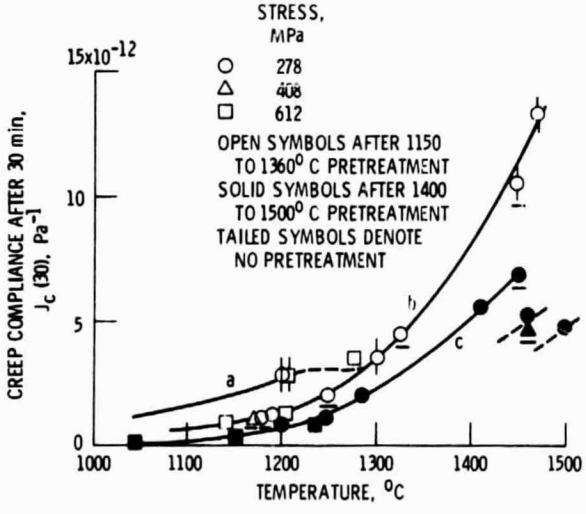

Figure 4. - Temperature, stress, and pretreatment dependence for the 30 min fiber creep compliance. Underlined data are for the SCS-6 fibers.

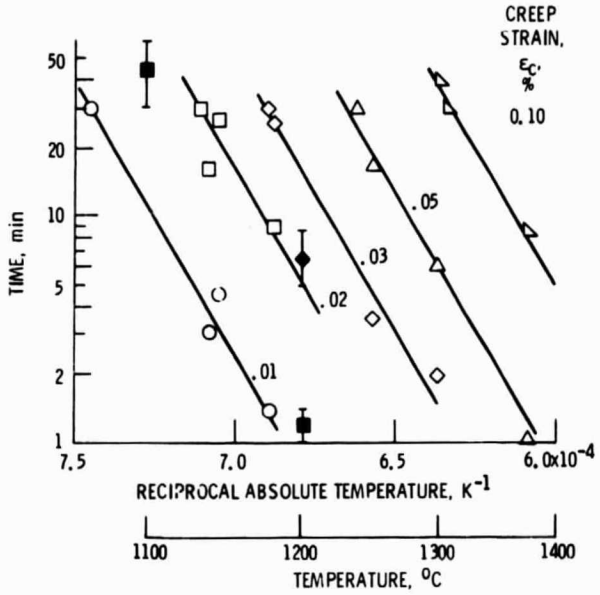

Figure 5. - Time to reach various levels of fiber creep strain as function of reciprocal absolute temperature (at 278 MPa stress). Solid points are from Ref. 20 for bulk siliconized SiC (at 303 MPa stress).

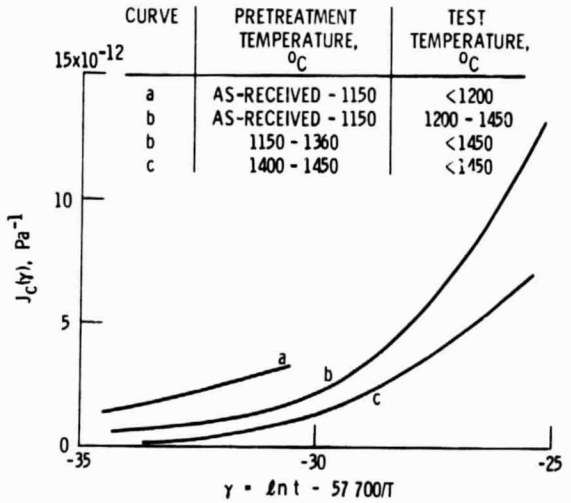

Figure 6. - Functional dependence of the CVD SiC fiber creep compliance J_c on the relaxation parameter γ (t is in seconds and T is in kelvin).

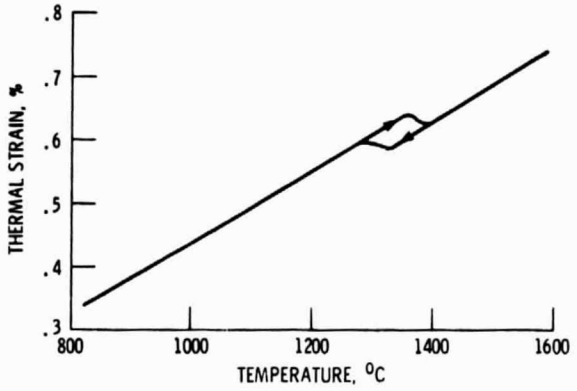

Figure 7. - Thermal expansion strain for CVD SiC fibers.

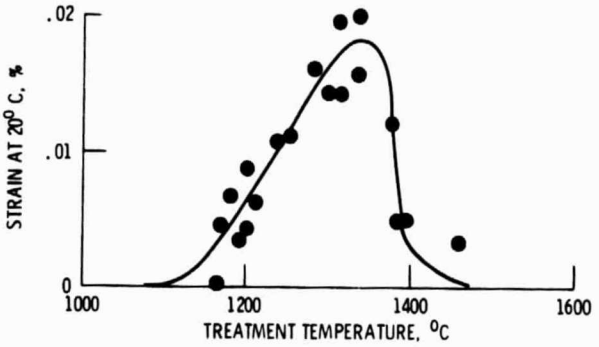

Figure 8. - Residual strain in CVD SiC fibers observed at 20° C after 30 min thermal treatment and quenching from the indicated temperatures.

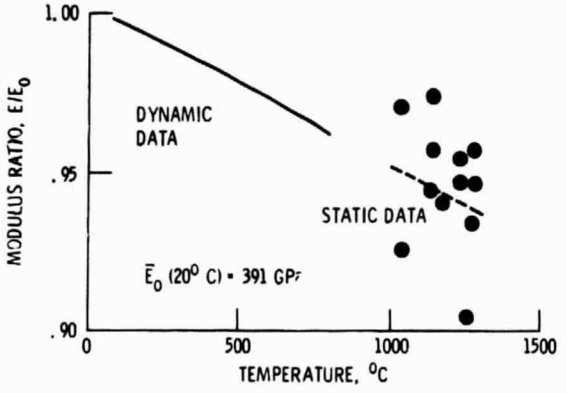

Figure 9. - Temperature dependence for the elastic Young's modulus of CVD SiC fibers.